

A new GPS velocity field for the Pacific Plate – Part 2: implications for fault slip rates in western California

C. DeMets,¹ Bertha Márquez-Azúa² and Enrique Cabral-Cano³

¹*Department of Geoscience, University of Wisconsin-Madison, Madison, WI 53706, USA. E-mail: chuck@geology.wisc.edu*

²*Centro Universitario de Ciencias Sociales y Humanidades, Universidad de Guadalajara, Guadalajara, Jalisco 44660, Mexico*

³*Departamento de Geomagnetismo y Exploración, Instituto de Geofísica, Universidad Nacional Autónoma de México, Ciudad Universitaria, 04510 México, D.F., Mexico*

Accepted 2014 September 5. Received 2014 September 3; in original form 2014 August 15

SUMMARY

Lower and upper bounds for present deformation rates across faults in central California between the San Andreas Fault and Pacific coast are estimated from a new Global Positioning System (GPS) velocity field for central, western California in light of geodetic evidence presented in a companion paper for slow, but significant deformation within the Pacific Plate between young seafloor in the eastern Pacific and older seafloor elsewhere on the plate. Transects of the GPS velocity field across the San Andreas Fault between Parkfield and San Juan Bautista, where fault slip is dominated by creep and the velocity field thus reveals the off-fault deformation, show that GPS sites in westernmost California move approximately parallel to the fault at an average rate of $3.4 \pm 0.4 \text{ mm yr}^{-1}$ relative to the older interior of the Pacific Plate, but only $1.8 \pm 0.6 \text{ mm yr}^{-1}$ if the Pacific Plate frame of reference is corrected for deformation within the plate. Modelled interseismic elastic deformation from the weakly coupled creeping segment of the San Andreas Fault is an order-of-magnitude too small to explain the southeastward motions of coastal sites in western California. Similarly, models that maximize residual viscoelastic deformation from the 1857 Fort Tejon and 1906 San Francisco earthquakes mismatch both the rates and directions of GPS site motions in central California relative to the Pacific Plate. Neither thus explains the site motions southwest of the San Andreas fault, indicating that the site motions measure deformation across faults and folds outboard of the San Andreas Fault. The non-zero site velocities thus constitute strong evidence for active folding and faulting outboard from the creeping segment of the San Andreas Fault and suggest limits of $0\text{--}2 \text{ mm yr}^{-1}$ for the Rinconada Fault slip rate and 1.8 ± 0.6 to $3.4 \pm 0.4 \text{ mm yr}^{-1}$ for the slip rates integrated across near-coastal faults such as the Hosgri, San Gregorio and San Simeon faults.

Key words: Satellite geodesy; Intraplate processes; Neotectonics; North America.

1 INTRODUCTION

Although the San Andreas Fault is widely recognized as the primary earthquake hazard in California, the $M_w = 6.5$ 2003 December 22 San Simeon earthquake was a reminder that faults in west-central California also threaten people and critical infrastructure, including the Diablo Canyon nuclear power plant (Fig. 1). To better understand the hazards posed by faults in the region, numerous geological and geophysical studies of faults such as the onland Rinconada fault and the mostly underwater Hosgri, San Gregorio and San Simeon faults (Fig. 2) have estimated their total offsets and long-term slip rates (e.g. Dickinson *et al.* 2005; Titus *et al.* 2007; Langenheim *et al.* 2013). Geodetic measurements have also proven critical for estimating individual fault slip rates in central California (e.g. Sauber *et al.* 1989; Savage *et al.* 1999) and testing hypotheses

about the mechanisms by which fault slip is accommodated during all phases of the earthquake cycle (e.g. Lisowski *et al.* 1991; Chuang & Johnson 2011).

Geodetic studies of deformation in western California have long referenced the velocities of sites in the region to the Pacific Plate (e.g. Argus *et al.* 1999; Beavan *et al.* 2002; McCaffrey 2005; Rolandone *et al.* 2008; Titus *et al.* 2011), which is the frame of reference most suitable for such studies. Ideally, estimates of Pacific Plate motion immediately offshore from California would be constrained by Global Positioning System (GPS) measurements at Pacific Plate sites close to California, but far enough to fall outside the region that is affected by distributed interseismic and post-seismic deformation associated with the San Andreas Fault and other faults in western California. To cope with the near-absence of such measurements, previous authors (cited above) have either

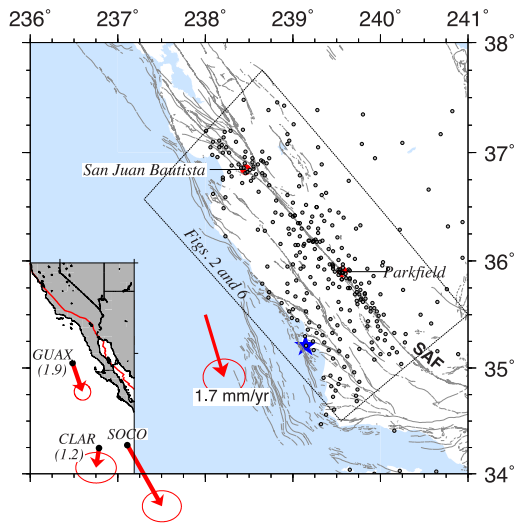


Figure 1. Study area in central and western California including geographic features referred to in the text. Grey circles indicate locations of GPS sites used for the analysis. Red arrow shows the average velocity and its 2-D, 1σ uncertainty for the GPS sites on Clarion and Guadalupe islands relative to the Pacific Plate interior. Blue star shows location of the Diablo Canyon nuclear power plant referred to in the text. ‘SAF’ labels the San Andreas Fault. The inset map locates GPS sites on Clarion (CLAR), Guadalupe (GUAX) and Socorro (SOCO) islands relative to the study area. The site velocities relative to the Pacific Plate are given in parentheses in units of millimetres per year (DeMets *et al.* 2014). No rate is given for SOCO because the motions of the GPS site and a nearby DORIS site are influenced by volcanic deformation (Briole *et al.* 2009; DeMets *et al.* 2014).

estimated the motion of the Pacific Plate from GPS sites that are located in the central, western, and southern Pacific, some 4000–10 000 km from western California or have estimated and corrected for the elastic effects of plate boundary deformation on sites nominally on the Pacific Plate in or near western California (McCaffrey 2005). The former approach leaves unresolved whether deformation occurs between areas of the Pacific Plate that are offshore from California and more distant areas of the plate and if so, how the intraplate deformation affects geodetic estimates of fault slip rates in and near western California. The latter approach introduces a model-dependent correction into the estimate of the Pacific Plate angular velocity.

In the first part of our two-part study of the Pacific Plate GPS velocity field (DeMets *et al.* 2014), we describe new geodetic measurements from GPS sites on Clarion, Guadalupe and Socorro islands (Fig. 1), which are the only islands on the eastern portion of the Pacific Plate where GPS measurements are logistically feasible and that are far enough from nearby plate boundary faults (800–2000 km) to be unaffected by their interseismic and postseismic deformation. We demonstrate that all three islands, which are on seafloor younger than 15 Myr, move SSE to SSW at rates of 1.0–4.3 mm yr^{-1} in a frame of reference that is defined by the velocities of 26 continuous GPS sites on islands in the central, southern, and western Pacific (inset to Fig. 1), where seafloor is 30–180-Myr-old. Excluding the more rapid motion of the Socorro Island GPS site, which is influenced by volcanic deformation (Briole *et al.* 2009; DeMets *et al.* 2014), the $1.7 \pm 0.6 \text{ mm yr}^{-1}$, $\text{S}17^\circ\text{E} \pm 11^\circ$ average motion of Clarion and Guadalupe islands relative to the plate interior constitutes the strongest evidence to date for deformation within the Pacific Plate.

Here, we exploit the above results to revisit the important question of how much deformation occurs in central California west of the San Andreas Fault, with emphasis on the present slip rates for faults that are located along and close to the coast. Our work is based on an analysis of the velocities of ≈ 300 GPS sites from central California, most located adjacent to and/or west of the ≈ 170 -km-long creeping segment of the central San Andreas Fault (Figs 1 and 2), where slip is accommodated primarily by aseismic creep (Burford & Harsh 1980). Unlike locked segments of the San Andreas Fault to the north and south of the creeping segment, where interseismic elastic deformation complicates efforts to quantify deformation that occurs off the fault, little or no interseismic elastic deformation affects the crust adjacent to much of the creeping segment (Rolandone *et al.* 2008; Ryder & Burgmann 2008; Titus *et al.* 2011). As a consequence, geodetic measurements along the creeping segment are more easily interpreted in the context of deformation that occurs in the borderlands of the San Andreas Fault, which we take advantage of in this analysis. We also consider whether the slow movements of GPS sites in western California relative to both Pacific Plate reference frames that we consider could be transient post-seismic effects of the 1857 Fort Tejon and/or 1906 San Francisco $M \sim 8$ earthquakes.

2 GPS DATA AND DATA ANALYSIS

Measurements from ≈ 300 sites in western California are used for the analysis (Fig. 1), including ≈ 200 continuously operating stations and ≈ 100 campaign and quasi-continuous GPS stations. The data, which span the period 1993 January 1 to 2014 late January, were procured from the U.S. Geological Survey, UNAVCO, the National Geodetic Survey and SOPAC. Further information about these sites is found in the Supporting Information.

Details of the GPS data analysis are given by DeMets *et al.* (2014) and are summarized only briefly here. All GPS data used in this study were processed with release 6.2 of the GIPSY software suite from the Jet Propulsion Laboratory (JPL). Daily GPS station coordinates were first estimated using a no-fiducial, precise point-positioning strategy (Zumberge *et al.* 1997), after which daily station positions were transformed to ITRF08 (Altamimi *et al.* 2011). Best-fitting station velocities were estimated via a weighted linear regression of the station position time-series, as were any offsets due to earthquakes or other factors such as GPS hardware changes. The coordinate time-series for some sites were affected by one or both of the $M_w = 6.5$ 2003 December 22 San Simeon and $M_w = 6.0$ 2004 September 28 Parkfield earthquakes and their post-seismic transient deformations. Methods for minimizing the effects of the two earthquakes on the estimated GPS site velocities are described in the electronic supplement and entail either judicious use of data from before and well after the earthquakes to avoid their effects or *a priori* corrections to GPS site positions to compensate for the coseismic and post-seismic effects of the earthquakes. Site velocity uncertainties were estimated using the method of Mao *et al.* (1999), which uses information about the length of a station time-series and the magnitudes of its white, flicker and random walk noise to estimate realistic site velocity uncertainties. The station velocities in ITRF08 and their uncertainties are given in Table S1.

3 RESULTS

Fig. 2 shows two realizations of the GPS velocity field of west-central California based on alternative frames of reference. In one

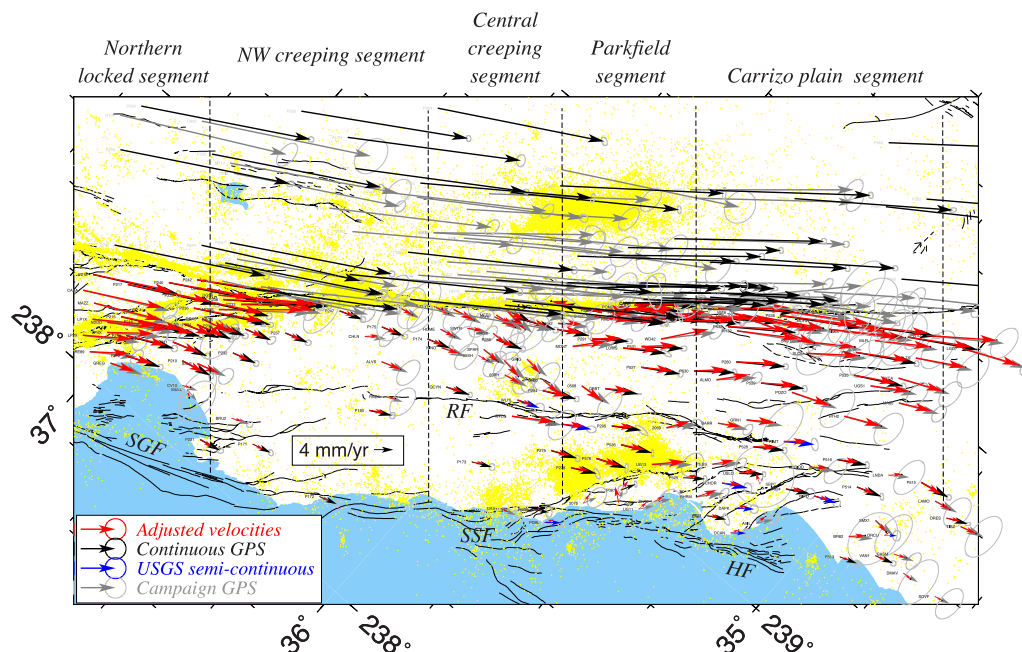


Figure 2. Oblique Mercator projection of central and western California with GPS site velocities relative to the Pacific Plate as defined by the motions of 26 GPS sites in the central, western, and southern Pacific (black, blue and grey arrows). Correcting the Pacific Plate frame of reference by the weighted average GPS velocity for Clarion and Guadalupe islands (Fig. 1) reduces the velocities of sites west of the San Andreas Fault (red arrows). The map, whose location is shown in Fig. 1, is projected such that the $\approx N41^\circ W$ trace of the San Andreas fault in central California is horizontal on the map. Yellow circles show the locations of earthquake epicentres for 1972–2009 from the Northern California Earthquake Data Centre catalogue. Velocity ellipses are 2-D, 1σ . The code for each site is visible upon magnification of the figure. Vertical dashed lines define the geographic limits of the five segments of the San Andreas Fault discussed in the text and shown in subsequent figures. Fault name abbreviations: HF, Hosgri fault; SGF, San Gregorio fault; SSF, San Simeon fault.

realization, shown by the black, blue and grey arrows in the figure, each GPS site velocity has been reduced by the motion of the Pacific Plate predicted at the site by an angular velocity that best fits the velocities of 26 Pacific Plate GPS sites that are 4000 km or farther from western California (table 2 in DeMets *et al.* 2014). The other realization, indicated by the red arrows in the figure, removes an additional $1.7 \pm 0.6 \text{ mm yr}^{-1}$ towards $S17^\circ E \pm 11^\circ$ from each site velocity, representing the weighted average velocity for the GPS sites on Clarion and Guadalupe islands relative to the Pacific Plate interior. The velocities depicted in the former frame of reference define the pattern of deformation between the San Andreas Fault and seafloor just west of California assuming that the Pacific Plate is rigid between areas offshore from California and the plate interior several thousand kilometres away. The latter assumes that the motions of Clarion and Guadalupe islands 800–2000 km south of western California record deformation between the plate interior and western California and corrects site velocities in California accordingly.

In both frames of reference, GPS site velocities in areas west of the creeping segment of the San Andreas Fault are typically 5 mm yr^{-1} or slower (Fig. 2). The slow, but non-zero motions of the sites relative to the Pacific Plate are most likely caused by distributed deformation (folding and faulting) in the fault borderlands (Titus *et al.* 2011), but may also include transient viscoelastic deformation from the $M_w = 7.9$ 1857 Fort Tejon earthquake (Hearn *et al.* 2013) and the $M \approx 8$ 1906 San Francisco earthquake and elastic strain from partially locked areas of the creeping segment (Rolandone *et al.* 2008; Ryder & Burgmann 2008). We consider each of these later in the analysis.

Fig. 3 subdivides the GPS velocity field of central California into five 50- to 80-km-wide transects orthogonal to the San Andreas Fault

(delineated in Fig. 2). The transects clearly show the variations in the pattern of geodetic velocities along the San Andreas Fault between northern California and the Carrizo Plain that have been described by many previous authors (e.g. Lisowski *et al.* 1991; Tong *et al.* 2013). Within the northernmost transect (Fig. 3a), which extends inland from Monterey Bay, and the southernmost transect (Fig. 3i), which includes the Carrizo Plain, strong velocity gradients on both sides of the fault and the absence of a sudden velocity change at the fault are evidence for strong locking of both fault segments (e.g. Lisowski *et al.* 1991; Tong *et al.* 2013). Estimating the slip rates for one or more additional active faults adjacent to the San Andreas fault within either of these transects, including the coastal and offshore faults of interest here, would entail discriminating the elastic velocity gradient for each fault from that of the San Andreas Fault. Such an effort would be challenging given the trade-offs in fit that occur between the fitted parameters, including the fault slip rates, their locking depths, and heterogeneities in their degree of coupling (e.g. Meade & Hager 2005).

In contrast to the strongly locked segments, transects of the GPS velocity field between San Juan Bautista and Parkfield (Figs 3c and e), where steady creep of the San Andreas Fault accommodates most motion between the Pacific Plate and Sierra Nevada–Great Valley (SNGV) block (Burford & Harsh 1980; Titus *et al.* 2005, 2006), exhibit sudden changes in the fault-parallel component of motion at the San Andreas Fault and weak velocity gradients on both sides of the fault. The weak velocity gradients and dominance of creep suggest there is little or possibly no elastic strain accumulation and hence coupling across this part of the San Andreas Fault. Enlarged views of the fault-parallel velocities for sites located between the Pacific coast and the two segments of the San Andreas Fault with the highest creep rates (Figs 4a–d) emphasize just how little the site

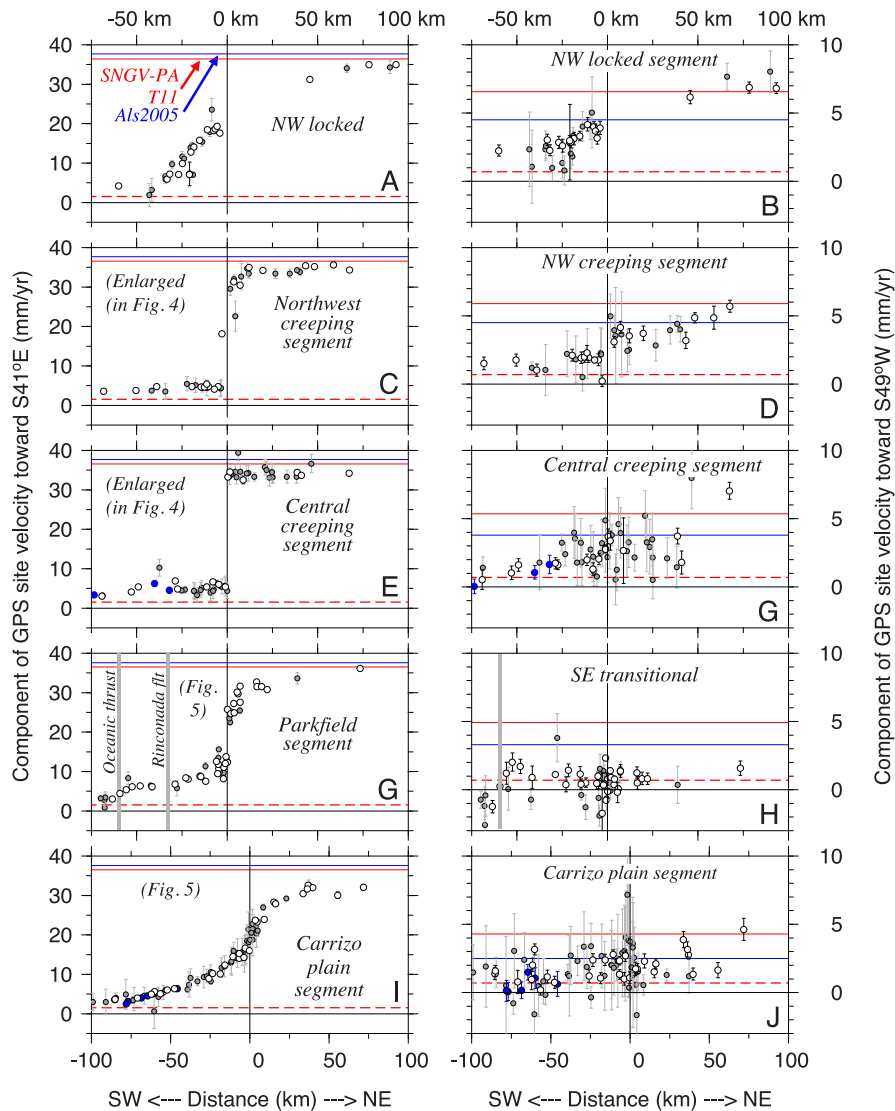


Figure 3. Transects of GPS velocity field from Fig. 2 with velocities rotated onto $S41^\circ E$ and $S49^\circ W$, approximately parallel and orthogonal to the San Andreas Fault of central California. Velocities are subdivided into the five fault-normal transects delineated in Fig. 2. Distances are measured southwest to northeast (left- to right-hand side) relative to the San Andreas Fault (0 km). Open, blue and grey circles are for continuous GPS velocities and velocities from quasi-continuous and campaign data, respectively. GPS velocities are relative to the Pacific Plate. The red dashed line shows the weighted residual velocity of Gaudalupe and Clarion islands rotated onto $S41^\circ E$ and $S49^\circ W$, representing a correction for potential Pacific Plate deformation described in the text. SNGV, Sierra Nevada-Great Valley; PA, Pacific; Als2005, d'Alessio *et al.* (2005); T11, Titus *et al.* (2011).

rates change with distance from the fault. Within both transects, the fault-parallel component of the site velocities decreases from $\sim 5 \text{ mm yr}^{-1}$ adjacent to the fault to $3\text{--}3.5 \text{ mm yr}^{-1}$ at the coast, a gradient of only 2 mm yr^{-1} across 70 km.

Finally, the Parkfield transect (Figs 3g and 5a), which is located between the locked and creeping segments of the fault, exhibits characteristics of both. The slip rate changes suddenly at the San Andreas Fault, similar to but less than the change in velocity along the creeping segment. The velocity gradient in the borderlands of the Parkfield segment is also intermediate between the weak and strong off-fault gradients associated with the creeping and locked segments, respectively. Velocities southwest of the Parkfield segment not only decrease monotonically towards the coast (Figs 5a and b), but also exhibit an inflection that is centered on the Oceanic and West Huasna faults, the former of which ruptured in the Dec. 22, 2003 $M_w = 6.5$ San Simeon earthquake. A similar inflection may be associated with the West Huasna fault southwest of the

Carrizo Plain segment (Fig. 5c), although it is more difficult to identify within the steeper velocity gradient associated with the strongly locked Carrizo Plain segment. Site velocities outboard of the Oceanic and West Huasna faults decrease to 3 mm yr^{-1} at the coast, similar to the slowest rates observed for coastal sites adjacent to the central and northwest creeping segments.

4 DISCUSSION

The results shown in Figs 2–5 unambiguously indicate that coastal and near-coastal GPS sites in coastal areas west of the creeping segment do not move with the Pacific Plate whether or not we correct the site velocities for possible deformation within the Pacific Plate. To better emphasize this point, Fig. 6 shows the velocities of all GPS sites that are located within a transect that extends along the coast $\sim 250 \text{ km}$ southeast from Monterey Bay. The nine GPS sites within this transect are located outboard from the creeping and Parkfield

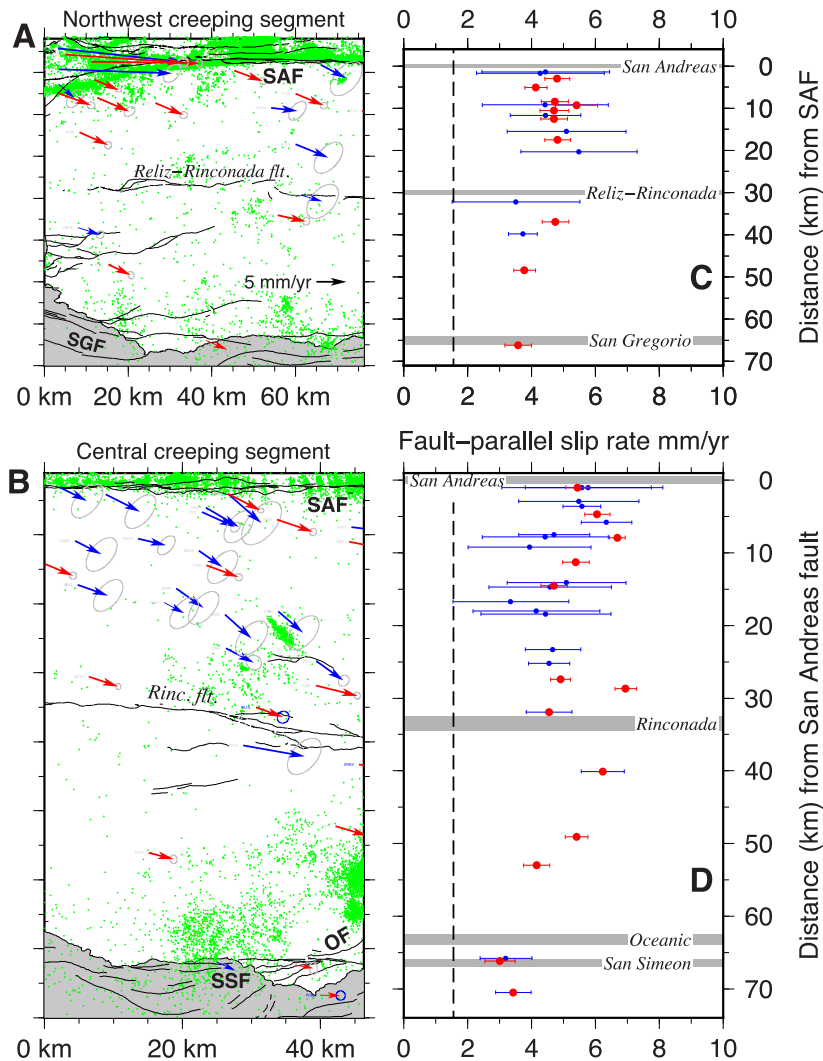


Figure 4. (a and b) Oblique Mercator projections of the northwest and central creeping segment transects delineated in Fig. 2 from the San Andreas Fault to the Pacific coast. Site velocities are relative to the Pacific Plate. Ellipses show 1σ , 2-D velocity uncertainties. Green dots are earthquakes. Red and blue arrows show the velocities for continuous and campaign GPS sites, respectively. Fault name abbreviations are ‘OF’, Oceanic fault; ‘SAF’, San Andreas Fault; ‘SGF’, San Gregorio fault; ‘SSF’, San Simeon fault. Panels (c) and (d) show velocities from (a) and (b) rotated onto $N41^\circ W$, the average strike of the San Andreas Fault, with distance from the San Andreas Fault. Panels (c) and (d) are aligned geographically with their corresponding maps (a) and (b). Zero motion indicates no fault-parallel movement relative to the Pacific Plate. The alternative Pacific Plate reference indicated by the black dashed line is the SAF-parallel component of the movements of Clarion and Guadalupe islands relative to the plate interior (see text). Relative to this reference frame, the fault-parallel motions of many coastal sites is reduced to an average of 1.8 mm yr^{-1} .

fault segments, where the elastic effects of locking along the San Andreas Fault should be small (see below). Those nine sites have fault-parallel rates that average $3.4 \pm 0.4 \text{ mm yr}^{-1}$ ($1\text{-}\sigma$) relative to the Pacific Plate, absent any correction for possible deformation within the plate, or $1.8 \pm 0.6 \text{ mm yr}^{-1}$ if Pacific Plate motion is corrected by the average motions of Clarion and Guadalupe islands (Fig. 6).

The $1.8\text{--}3.4 \text{ mm yr}^{-1}$ motions of the coastal and near-coastal sites have three possible causes. One is active faulting offshore from central California, the target of our analysis. A second is possible partial locking of the creeping segment of the San Andreas Fault or locking along other faults such as the Rinconada or offshore faults. Either would give rise to elastic slip deficits that would appear as southeastward, fault-parallel motions of sites in western California relative to the Pacific Plate. Finally, residual viscoelastic deformation from the 1857 Fort Tejon earthquake and/or the 1906

San Francisco earthquake may still influence present-day deformation in western California. We evaluate each of these possibilities below.

4.1 Elastic effects of partial locking of the creeping segment

We first estimate how much elastic deformation would result along the coast west of the creeping segment if the creeping segment were partially locked. From inversions of InSAR and GPS observations of active deformation adjacent to the creeping segment, Ryder & Burgmann (2008) and Rolandone *et al.* (2008) find evidence for partial (≈ 10 to ≈ 20 per cent) coupling of the San Andreas creeping segment above depths of 12 km. Conversely, Titus *et al.* (2011) argue that permanent deformation in the fault borderlands may account for

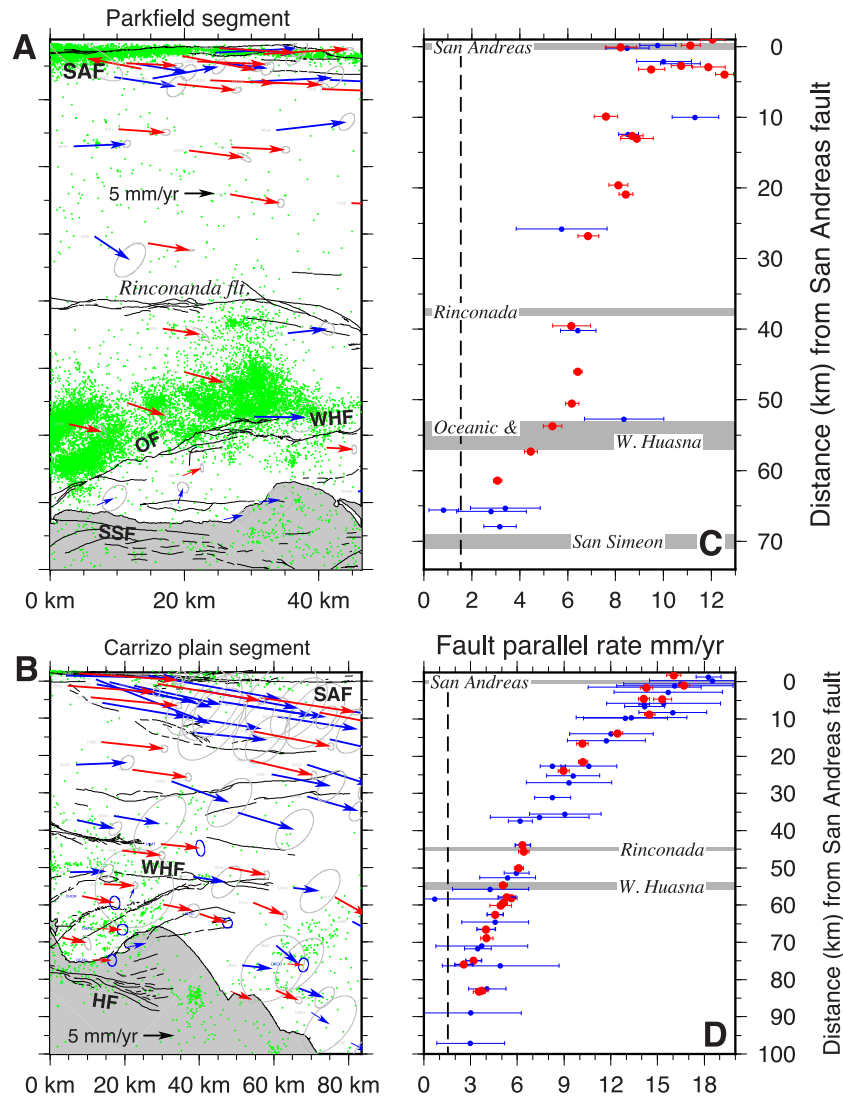


Figure 5. (a and b) Oblique Mercator projections of the southeast transitional and Carrizo Plain segment transects delineated in Fig. 2 from the San Andreas fault to the Pacific coast. See caption to previous figure for more information. Panels (c) and (d) show velocities from (a) and (b) rotated onto the trend of the San Andreas Fault, with distance from the San Andreas Fault. See previous figure caption for additional information. Fault name abbreviations are ‘HF’, Hosgri fault; ‘OF’, Oceanic fault; ‘SAF’, San Andreas Fault; ‘SSF’, San Simeon fault; ‘WHF’, West Huasnas fault.

all the deformation adjacent to the fault, in which case the creeping segment may be entirely uncoupled. These studies suggest lower and upper bounds of 0 and 20 per cent for possible coupling of the creeping segment. We calculated the elastic surface deformation in the borderlands of the San Andreas Fault for a simple homogeneous elastic half-space in which a vertical San Andreas Fault slips freely at 35 mm yr^{-1} below depths of 12 km and is coupled at 20 per cent above depths of 12 km, corresponding to Ryder & Burgmann’s (2008) preferred model for a partially locked creeping segment. The resulting deformation field southwest of the fault is dominated by a SE-directed elastic slip deficit that decreases from 2 mm yr^{-1} at locations near the fault to only 0.2 mm yr^{-1} at locations along the Pacific coast.

In order to further maximize elastic deformation southwest of the fault, we also incorporated a vertical Rinconada fault into our elastic model using an assumed maximum slip rate of 2 mm yr^{-1} (Rolandone *et al.* 2008) and locking depth of 15 km. The elastic slip deficits predicted by this model along the Pacific coast are also

no more than a few tenths of a millimetres per year. The combined elastic slip deficit for the San Andreas and Rinconada faults at coastal locations southwest of the creeping segment is no greater than 0.5 mm yr^{-1} relative to undeformed lithosphere several hundred km offshore from the coast. Given our modelling assumptions, any elastic slip deficit along the Pacific coast is likely to be no larger than 0.5 mm yr^{-1} and could easily be smaller than 0.1 mm yr^{-1} given the unknowns. The predicted elastic deformation is significantly smaller than the observed $1.8\text{--}3.4 \text{ mm yr}^{-1}$ velocities of GPS sites along the Pacific coast. We conclude that interseismic elastic deformation associated with locking of the San Andreas and possibly Rinconada faults cannot explain the observed site velocities.

4.2 Viscoelastic effects of 1857 and 1906 earthquakes

In order to approximate the viscoelastic effects of the $M_w = 7.9$ 1857 Fort Tejon and $M \sim 8$ 1906 San Francisco earthquakes during

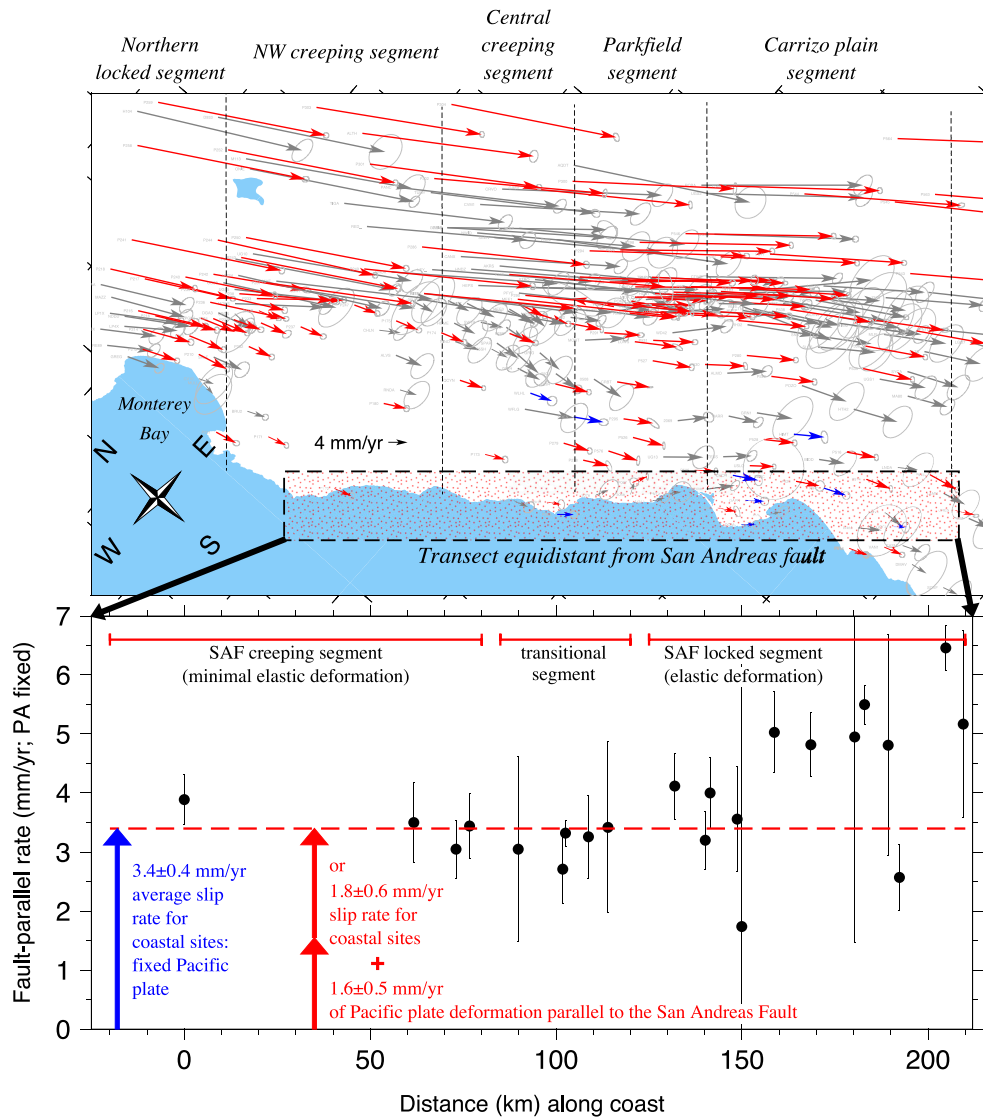


Figure 6. Component of site velocities parallel to the San Andreas Fault ($N41^\circ W$) of central California for GPS sites within a coastal transect equidistant from the San Andreas fault (shaded region of map). Frame of reference is the Pacific Plate as defined by the motions of 26 GPS stations in the central, western, and southern Pacific. The elastic effects from the locked San Andreas Fault are small or possibly nonexistent adjacent to the creeping segment (Titus *et al.* 2006, 2011; Ryder & Burgmann 2008). In those areas, the $3.4 \pm 0.4 \text{ mm yr}^{-1}$ average rate of the coastal sites may approximate the total slip rate across faults between the coastal GPS sites and undeforming Pacific Plate lithosphere farther offshore. Alternatively, the SAF-parallel slip rate across the same faults may be only $1.8 \pm 0.6 \text{ mm yr}^{-1}$ if the 1.7 mm yr^{-1} , SSE-directed motions of Clarion and Guadalupe islands are taken as evidence that Pacific Plate lithosphere offshore from California moves relative to the Pacific Plate interior.

the period spanned by the GPS measurements used in this study (1994–2014), we used Visco-1D software (version 3; Pollitz 1997) to predict a maximum viscoelastic response to each earthquake. We use crustal model M1 of Hearn *et al.* (2013) to approximate the layered viscosity structure in California. This viscosity structure assumes a relatively low viscosity of $3 \times 10^{18} \text{ Pa s}$ for the mantle below depths of 50 km, which gives rise to more rapid surface deformation than viscosity structures with higher viscosity mantles. For the 1906 San Francisco earthquake, we adopt the fault slip solution of Thatcher *et al.* (1997), which subdivides the $\sim 500\text{-km}$ -long rupture zone into 48 segments with coseismic slips ranging from 225 to 860 cm (see Fig. S1 for this paper and table 1 of Thatcher *et al.* 1997). For the 1857 Fort Tejon earthquake, we adopt Zielke *et al.*'s (2010) slip solution, which features

an average of 5.3 m of slip along a $\sim 300\text{-km}$ -long rupture zone (see Fig. S2).

For the 1906 earthquake, the predicted viscoelastic deformation within our study area for the period 1994–2014 implies 20-yr-average velocity perturbations that are dominantly orthogonal to the San Andreas Fault (Fig. S1) and that average only 0.2 mm yr^{-1} along the coast. The predicted viscoelastic deformation is perpendicular to the observed $2\text{--}3.4 \text{ mm yr}^{-1}$ fault-parallel motions of the coastal and near-coastal GPS sites and is an order-of-magnitude slower than the observed velocities.

The viscoelastic velocity perturbations predicted for the 1857 Fort Tejon earthquake also fail to match the observed GPS site velocities. The viscoelastic velocities that are predicted for sites southwest of the San Andreas fault along the central and

northwest sections of the creeping segment are orthogonal to the fault (Fig. S2) and average only 0.1 mm yr^{-1} along much of the coast. Our results corroborate those reported by Hearn *et al.* (2013) for this earthquake.

We conclude that any residual viscoelastic component of the present GPS velocity field from the 1857 and 1906 earthquakes is negligible in our study area and is too small to explain the $1.8\text{--}3.4 \text{ mm yr}^{-1}$ fault-parallel motions of GPS sites along the Pacific coast.

4.3 Upper and lower fault slip-rate estimates

Given that neither elastic nor viscoelastic deformation is rapid enough nor in the right direction to explain the $1.8\text{--}3.4 \text{ mm yr}^{-1}$ southeast-directed motions of coastal GPS sites in central California, a tectonic explanation is called for, most likely consisting of some combination of distributed folding and faulting outboard from the creeping segment. If faulting accommodates most of the deformation, as seems more likely, the most obvious candidates include the Rinconada fault and offshore faults such as the San Simeon fault zone, the San Gregorio fault near and southeast of Monterey Bay, and possibly the Hosgri fault south of the western termination of the Oceanic fault (Figs. 4a and c).

Eight of the nine GPS sites that are located within the coastal transect depicted in Fig. 6 have velocities that agree within $\pm 0.5 \text{ mm yr}^{-1}$ of their mean value. If no deformation occurs within the Pacific Plate, the component of these nine site velocities parallel to the San Andreas Fault has an average value of $3.4 \pm 0.4 \text{ mm yr}^{-1}$. We consider this an upper limit for the margin-parallel component of the slip rate for faults near the coast. Alternatively, if we assume the Pacific Plate deforms and reduce the velocities of the nine sites by the $1.7 \pm 0.6 \text{ mm yr}^{-1}$, $S17^\circ E \pm 11^\circ$ average motion of Clarion and Guadalupe islands relative to the plate interior, the SAF-parallel component of the nine sites is reduced to $1.8 \pm 0.6 \text{ mm yr}^{-1}$ (1σ). This represents our best lower bound for the cumulative margin-parallel slip rate for faults near the coast.

Upper and lower bounds for the slip rate of the Rinconada fault, which is located midway between the Pacific coast and San Andreas Fault (Figs 4a and b), can be inferred as follows. We infer an upper bound of $\sim 2 \text{ mm yr}^{-1}$ by attributing the entire $1\text{--}2 \text{ mm yr}^{-1}$ velocity gradient southwest of the San Andreas Fault (Figs 4a and b) to presumed, distributed elastic deformation associated with locking of the Rinconada fault. Alternatively, if the velocity gradient instead records distributed folding and faulting along structures other than the Rinconada fault, as suggested by geological data (Titus *et al.* 2011), the Rinconada fault may be completely inactive. The bounds on the likely slip rate for the Rinconada fault are thus $0\text{--}2 \text{ mm yr}^{-1}$, consistent with a previous, GPS-derived estimate (Rolandone *et al.* 2008).

4.4 Comparison to independent geological and geodetic slip rate estimates

Geological and seismological observations indicate that the San Gregorio and San Simeon faults have been active during the Holocene. Trenching across onland portions of the San Simeon fault, which connects the the San Gregorio and Hosgri faults (Fig. 2), gives a Holocene slip rate of $0.9\text{--}3.4 \text{ mm yr}^{-1}$ and best estimate of $1.0\text{--}1.4 \text{ mm yr}^{-1}$ (Hall *et al.* 1994), similar to a $1\text{--}3 \text{ mm yr}^{-1}$ geologically derived estimate near San Simeon (Hanson *et al.* 2004). These agree with our GPS-derived lower and upper bounds of 1.8 ± 0.6 and $3.4 \pm 0.4 \text{ mm yr}^{-1}$.

Our estimated slip-rate limits also agree with most though not all previously published slip-rate estimates for the San Gregorio and Hosgri faults from modelling of GPS observations. In particular, our lower and upper slip-rate bounds are consistent with results reported by d'Alessio *et al.* (2005), who predict $2.4 \pm 1 \text{ mm yr}^{-1}$ of dextral slip, McCaffrey (2005), who predicts $2.6 \pm 2 \text{ mm yr}^{-1}$ on the San Gregorio fault south of Monterey Bay and $1.5\text{--}3.5 \text{ mm yr}^{-1}$ on the Hosgri fault, and Johnson & Fukuda (2010), who variously predict $1\text{--}5 \text{ mm yr}^{-1}$ or $3\text{--}5 \text{ mm yr}^{-1}$ for the San Gregorio fault depending on their underlying model assumptions. Conversely, our estimates differ significantly from those estimated by Bird (2009), who predict a slip rate of 0.8 mm yr^{-1} for the San Gregorio fault, and Rolandone *et al.* (2008), who predict a $4.3\text{--}5.3 \text{ mm yr}^{-1}$ slip rate for the San Gregorio/Hosgri fault system.

5 CONCLUSIONS

An analysis of a new GPS velocity field for central California in two frameworks for the Pacific Plate, one defined by the GPS velocities of 26 stations in the central, western and southern Pacific and the other including a correction for 1.7 mm yr^{-1} of SSE-directed intraplate deformation indicated by newly available GPS measurements on islands in the eastern Pacific basin, indicates that GPS sites in western California outboard from the creeping segment of the San Andreas Fault move southeastward parallel to the fault at average rates of either 1.8 ± 0.6 or $3.4 \pm 0.4 \text{ mm yr}^{-1}$ depending on which reference frame is adopted. Any elastic effects from locking of the San Andreas Fault in this region are too small to explain the observed slip deficits at sites along the coast given that creep accommodates most or all slip along the San Andreas Fault in this region. Perturbations to the velocity field due to viscoelastic effects of the 1857 Fort Tejon and 1906 San Francisco earthquakes are too small and in the wrong direction to explain the observed coastal and near-coastal site motions. We thus attribute all of the GPS-measured deformation southwest of the creeping segment of the San Andreas Fault to faulting and folding and estimate lower and upper limits for present-day slip rates along near-coastal faults of 1.8 ± 0.6 or $3.4 \pm 0.4 \text{ mm yr}^{-1}$, respectively. The lower bound differs significantly from zero, indicating that near-coastal faults are still active, in accord with geological and seismic observations.

ACKNOWLEDGEMENTS

This work originated as an effort to quantify seismic hazard in western California from the perspective of the Pacific Plate. It was funded partly by Pacific Gas and Electric. Support for this project was also provided by UNAM's PAPIT project IN104213-2 and National Science Foundation grant EAR-1114174. We thank Paul Tregoning and Saskia Goes for their constructive reviews. We thank Jesse Murray, Wayne Thatcher, and Jerry Svarc of the U.S. Geological Survey for making their quasi-continuous and campaign GPS data for California available for our analysis. Readers may also refer to www.earthquake.usgs.gov/monitoring/gps/CentralCalifornia_SGPS/ for up-to-date information about this region. Figures were drafted using Generic Mapping Tools software (Wessel & Smith 1991). We are grateful for open access to continuous GPS data from the Plate Boundary Observatory operated by UNAVCO and supported by National Science Foundation grants EAR-0350028 and EAR-0732947 and the Global GNSS Network operated by UNAVCO for NASA Jet Propulsion Laboratory under NSF Cooperative Agreement No. EAR-0735156.

REFERENCES

- Altamimi, Z., Collilieux, X. & Metivier, L., 2011. ITRF2008: an improved solution of the international terrestrial reference frame, *J. Geod.*, **85**, 457–473.
- Argus, D.F. *et al.*, 1999. Shortening and thickening of metropolitan Los Angeles measured by using geodesy, *Geology*, **27**, 703–706.
- Beavan, J., Tregoning, P., Bevis, M., Kato, T. & Meertens, C., 2002. Motion and rigidity of the Pacific plate and implications for plate boundary deformation, *J. geophys. Res.*, **107**(B10), doi:10.1029/2001JB000282.
- Bird, P., 2009. Long-term fault slip rates, distributed deformation rates, and forecast of seismicity in the western United States from joint fitting of community, geologic, geodetic, and stress direction data sets, *J. geophys. Res.*, **114**, B11403, doi:10.1029/2009JB006317.
- Briole, P., Willis, P., Dubois, J. & Charade, O., 2009. Potential volcanological applications of the DORIS system: a geodetic study of the Socorro Island (Mexico) coordinate time series, *Geophys. J. Int.*, **178**, 581–590.
- Burford, R.O. & Harsh, P.W., 1980. Slip on the San Andreas Fault in central California from alignment array surveys, *Bull. seism. Soc. Am.*, **70**, 1233–1261.
- Chuang, R.Y. & Johnson, K.M., 2011. Reconciling geologic and geodetic model fault slip-rate discrepancies in Southern California: consideration of nonsteady mantle flow and lower crustal fault creep, *Geology*, **39**, 627–630.
- d’Alessio, M.A., Johanson, I.A., Burgmann, R., Schmidt, D. & Murray, M.H., 2005. Slicing up the San Francisco Bay Area: block kinematics and fault slip rates from GPS-derived surface velocities, *J. geophys. Res.*, **110**, B06403, doi:10.1029/2004JB003496.
- DeMets, C., Márquez-Azúa, B. & Cabral-Cano, E., 2014. A new GPS velocity field for the Pacific Plate – Part 1: constraints on plate motion, intraplate deformation, and the viscosity of Pacific basin asthenosphere, *Geophys. J. Int.*, doi:10.1093/gji/ggu341.
- Dickinson, W.R. *et al.*, 2005. Net dextral slip, Neogene San Gregorio-Hosgri fault zone, coastal California: geologic evidence and tectonic implications, *GSA Special Paper*, **391**, 1–43.
- Hall, N.T., Hunt, T.D. & Vaughan, P.R., 1994. Holocene behavior of the San Simeon fault zone, south-central coastal California, *GSA Special Paper*, **292**, 167–190.
- Hanson, K.L., Lettis, W.R., McLaren, M.K., Savage, W.U. & Hall, T.N., 2004. Style and rate of Quaternary deformation of the Hosgri fault zone, *Offshore south-central California*, U.S. Geological Survey Bulletin, 1995-BB, 37 pp.
- Hearn, E.H., Onishi, C.T., Pollitz, F.F. & Thatcher, W.R., 2013. How do “ghost transients” from past earthquakes affect GPS slip rate estimates on southern California faults?, *Geochem. Geophys. Geosys.*, **14**, doi:10.1002/ggge.20080.
- Johnson, K.M. & Fukuda, J., 2010. New methods for estimating the spatial distribution of locked asperities and stress-driven interseismic creep on faults with application to the San Francisco Bay Area, California, *J. geophys. Res.*, **115**, B12408, doi:10.1029/2010JB007703.
- Langenheim, V.E., Jachens, R.C., Graymer, R.W., Colgan, J.P., Wentworth, C.M. & Stanley, R.G., 2013. Fault geometry and cumulative offsets in the central Coast Ranges, California: evidence for northward increasing slip along the San Gregorio-San Simeon-Hosgri fault, *Lithosphere*, **5**, 29–48.
- Lisowski, M., Savage, J.C. & Prescott, W.H., 1991. The velocity field along the San Andreas Fault, *J. geophys. Res.*, **96**, 8369–8389.
- Mao, A., Harrison, C.G.A. & Dixon, T.H., 1999. Noise in GPS coordinate time series, *J. geophys. Res.*, **104**, 2797–2816.
- McCaffrey, R., 2005. Block kinematics of the Pacific-North America plate boundary in the southwestern United States from inversion of GPS, seismological, and geologic data, *J. geophys. Res.*, **110**, B07401, doi:10.1029/2004JB003307.
- Meade, B.J. & Hager, B.H., 2005. Block models of crustal motion in southern California constrained by GPS measurements, *J. geophys. Res.*, **110**, B03403, doi:10.1029/2004JB003209.
- Pollitz, F.F., 1997. Gravitational viscoelastic postseismic relaxation on a layered spherical Earth, *J. geophys. Res.*, **102**, 17 921–17 941.
- Rolandone, F. *et al.*, 2008. Aseismic slip and fault-normal strain along the central creeping section of the San Andreas Fault, *Geophys. Res. Lett.*, **35**, L14305, doi:10.1029/2008GL034437.
- Ryder, I. & Burgmann, R., 2008. Spatial variations in slip deficit on the central San Andreas Fault from InSAR, *Geophys. J. Int.*, **175**, 837–852.
- Sauber, J., Lisowski, M. & Solomon, S.C., 1989. Geodetic measurements of deformation east of the San Andreas Fault in central California, in *Slow Deformation and Transmission of Stress in the Earth*, *Geophys. Monogr. Ser.*, Vol. 49, pp. 71–86, eds Cohen, S.C. & Vanicek, P., AGU.
- Savage, J.C., Svarc, J.L. & Prescott, W.H., 1999. Geodetic estimates of fault slip rates in the San Francisco Bay area, *J. geophys. Res.*, **104**, 4995–5002.
- Thatcher, W., Marshall, G. & Lisowski, M., 1997. Resolution of fault slip along the 470-km-long rupture of the great 1906 San Francisco earthquake and its implications, *J. geophys. Res.*, **102**, 5353–5367.
- Titus, S.J., DeMets, C. & Tikoff, B., 2005. New slip rate estimates for the creeping segment of the San Andreas Fault, *Geology*, **33**, 205–208.
- Titus, S.J., DeMets, C. & Tikoff, B., 2006. Thirty-five-year creep rates for the creeping segment of the San Andreas Fault and the effects of the 2004 Parkfield earthquake: constraints from alignment arrays, continuous Global Positioning System, and creepmeters, *Bull. seism. Soc. Am.*, **96**, S250–S268.
- Titus, S.J., Housen, B. & Tikoff, B., 2007. A kinematic model for the Rinconada fault system in central California based on structural analysis of *en echelon* folds and paleomagnetism, *J. Struct. Geol.*, **29**, 961–982.
- Titus, S.J., Dyson, M., DeMets, C., Tikoff, B., Rolandone, F. & Bürgmann, R., 2011. Geologic versus geodetic deformation adjacent to the San Andreas Fault, central California, *Geol. soc. Am. Bull.*, **123**, 794–820.
- Tong, X., Sandwell, D.T. & Smith-Konter, B., 2013. High-resolution interseismic velocity data along the San Andreas Fault from GPS and InSAR, *J. geophys. Res.*, **118**, doi:10.1029/2012JB009442.
- Wessel, P. & Smith, W.H.F., 1991. Free software helps map and display data, *EOS, Trans. Am. geophys. Un.*, **72**, 441–446.
- Zielke, O., Arrowsmith, J.R., Ludwig, L.G. & Akciz, S.O., 2010. Slip in the 1857 and earlier large earthquakes along the Carrizo Plain, San Andreas Fault, *Science*, **327**, 1119–1122.
- Zumberge, J.F., Heflin, M.B., Jefferson, D.C., Watkins, M.M. & Webb, F.H., 1997. Precise point positioning for the efficient and robust analysis of GPS data from large networks, *J. geophys. Res.*, **102**, 5005–5017.

SUPPORTING INFORMATION

Additional Supporting Information may be found in the online version of this article:

Figure S1. Viscoelastic deformation (red arrows) calculated for the April 18, 1906 San Francisco earthquake. Blue line shows the extent of the Thatcher *et al.* (1997) fault slip solution that is used to drive the viscoelastic model. Rheological model M1 from Hearn *et al.* (2013) is used to maximize the viscoelastic response to the earthquake. The grey box outlines the region in central California that is pertinent to this study. In order to facilitate the comparison to GPS velocities, the viscoelastic deformation was computed for the period 1994 to 2014, coinciding with the period of GPS observations used in this study, and converted to 20-yr-average velocities.

Figure S2. Viscoelastic deformation (red arrows) calculated for the January 9, 1857 Fort Tejon earthquake. Blue line shows the extent of the Zielke *et al.* (2010) fault slip solution that is used to drive the viscoelastic model. Rheological model M1 from Hearn *et al.* (2013) is used to maximize the viscoelastic response to the earthquake. The grey box outlines the region in central California that is pertinent to this study. In order to facilitate the comparison to GPS velocities, the viscoelastic deformation is computed for the period 1994 to 2014, coinciding with the period of GPS observations used in this study, and converted to 20-yr-average velocities.

Table S1. GPS station information.

Table S2. Campaign station earthquake offset information.
(<http://gji.oxfordjournals.org/lookup/suppl/doi:10.1093/gji/ggu347/-/DC1>).

Please note: Oxford University Press is not responsible for the content or functionality of any supporting materials supplied by the authors. Any queries (other than missing material) should be directed to the corresponding author for the article.